Monthly Notices
of the
ROYAL ASTRONOMICAL SOCIETY

Mon. Not. R. Astron. Soc. **412,** 2530–2542 (2011) doi:10.1111/j.1365-2966.2010.18076.x

External field effect of modified Newtonian dynamics in the Solar system

Luc Blanchet[1]★ and Jérôme Novak[2]★

[1]$\mathcal{GR}\varepsilon\mathbb{C}\mathcal{O}$, *Institut d'Astrophysique de Paris — UMR 7095 du CNRS, Université Pierre et Marie Curie, 98*[bis] *boulevard Arago, 75014 Paris, France*
[2]*Laboratoire Univers et Théories, Observatoire de Paris, CNRS, Université Paris Diderot, 5 place Jules Janssen, 92190 Meudon, France*

Accepted 2010 November 23. Received 2010 November 11; in original form 2010 October 6

ABSTRACT

The modified Newtonian dynamics (MOND) have been formulated as a modification of the Poisson equation for the Newtonian gravitational field. This theory generically predicts a violation of the strong version of the equivalence principle and as a result, the gravitational dynamics of a system depend on the external gravitational field in which the system is embedded. This so-called external field effect has been recently shown to imply the existence of an anomalous quadrupolar correction, along the direction of the external galactic field, in the gravitational potential felt by planets in the Solar system. In this paper, we confirm the existence of this effect by a numerical integration of the MOND equation in the presence of an external field and compute the secular precession of the perihelion of planets induced by this effect. We find that the precession effect is rather large for outer gaseous planets and in the case of Saturn, it is comparable to published residuals of precession obtained by Saturn range tracking data. The effect is much smaller for inner planets, but in the case of the Earth, it appears to be in conflict for most of the MOND functions $\mu(y)$ with the very good constraint on the perihelion precession obtained from Jupiter very long baseline interferometry data. The MOND functions that are compatible with this constraint appear to have a very rapid transition from the MONDian regime to the Newtonian one.

Key words: methods: numerical – planets and satellites: general – galaxies: kinematics and dynamics – dark matter.

1 INTRODUCTION

1.1 Motivation

The modified Newtonian dynamics (MOND) – Milgrom (1983a,b,c) – is a successful alternative framework for interpreting the galactic rotation curves and the empirical Tully–Fisher relation without relying on dark matter haloes (see Sanders & McGaugh 2002 for a review). At the non-relativistic level, the best-modified-gravity formulation of the MOND is the modified Poisson equation originally proposed by Bekenstein & Milgrom (1984):

$$\nabla\cdot\left[\mu\left(\frac{g}{a_0}\right)\nabla U\right]=-4\pi G\rho\,, \tag{1}$$

where ρ is the density of ordinary (baryonic) matter, U is the gravitational potential, $\boldsymbol{g}=\nabla U$ is the gravitational field and $g=|\boldsymbol{g}|$ its ordinary Euclidean norm. The modification of the Poisson equation is encoded in the MOND function $\mu(y)$ of the single argument $y\equiv g/a_0$, where $a_0=1.2\times10^{-10}\,\mathrm{m\,s^{-2}}$ denotes the MOND constant acceleration scale. The MOND function interpolates between the MOND regime corresponding to weak gravitational fields $y=g/a_0\ll1$, for which it behaves as $\mu(y)=y+o(y)$, and the Newtonian strong-field regime $y\gg1$, where μ reduces to 1 so that we recover the usual Newtonian gravity.

Relativistic extensions of MOND modifying general relativity have been proposed (Bekenstein 2004; Sanders 2005) and extensively studied (see Bekenstein 2005 for a review). Alternatively, MOND equation (1) can be reinterpreted as a modification of dark matter rather than gravity by invoking a mechanism of 'gravitational polarization' – a gravitational analogue of electric polarization (Blanchet 2007); this yields to the concept of dipolar dark matter which has been formulated as a relativistic model in standard general relativity by Blanchet & Le Tiec (2008, 2009).

An important consequence of the non-linearity of equation (1) in the MOND regime is that the gravitational dynamics of a system are influenced (besides the well-known tidal force) by the external gravitational environment in which the system is embedded. This is known as the external field effect (EFE), which has non-trivial implications for non-isolated gravitating systems. The EFE was conjectured to explain the dynamics of open star clusters in our galaxy (Milgrom 1983a,b,c), since they do not show evidence of dark matter, despite the involved weak internal accelerations (i.e. below a_0). The EFE effect shows that the dynamics of these systems should actually be Newtonian as a result of their immersion in the gravitational field of the Milky Way. The EFE is a rigorous prediction of Bekenstein–Milgrom equation (1) and is best exemplified by the asymptotic behaviour of the solution of equation (1) far from a

★E-mail: blanchet@iap.fr (LB); jerome.novak@obspm.fr (JN)

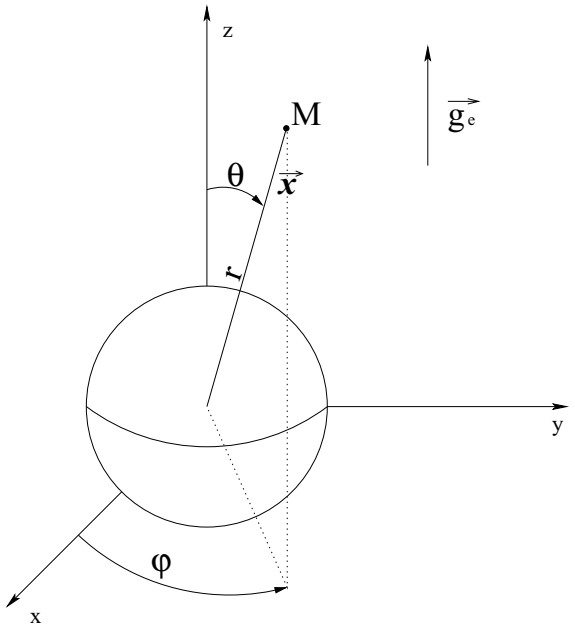

Figure 1. Setting of the spherically symmetric star and the asymptotic galactic field $\boldsymbol{g}_e$, using spherical coordinates $\{r, \theta, \varphi\}$.

localized matter distribution (say, the Solar system), in the presence of a constant external gravitational field $\boldsymbol{g}_e$ (the field of the Milky Way). At large distances, $r = |\boldsymbol{x}| \to \infty$, we have (Bekenstein & Milgrom 1984):

$$U = \boldsymbol{g}_\mathrm{e} \cdot \boldsymbol{x} + \frac{GM/\mu_\mathrm{e}}{r\sqrt{1+\lambda_\mathrm{e}\sin^2\theta}} + \mathcal{O}\left(\frac{1}{r^2}\right), \tag{2}$$

where M is the mass of the localized matter distribution, θ is the azimuthal angle from the direction of the external field $\boldsymbol{g}_\mathrm{e}$ (see also Fig. 1), and we denote $\mu_\mathrm{e} \equiv \mu(y_\mathrm{e})$ and $\lambda_\mathrm{e} \equiv y_\mathrm{e}\mu'_\mathrm{e}/\mu_\mathrm{e}$, with $y_\mathrm{e} = g_\mathrm{e}/a_0$ and $\mu'_\mathrm{e} = \mathrm{d}\mu\,(y_\mathrm{e})/\mathrm{d}y_\mathrm{e}$. In the presence of the external field, the MOND internal potential $u \equiv U - \boldsymbol{g}_\mathrm{e} \cdot \boldsymbol{x}$ shows a Newtonian-like fall-off $\sim r^{-1}$ at large distances but with an effective gravitational constant G/μ_e.[1] However, contrary to the Newtonian case, it exhibits a non-spherical deformation along the direction of the external field. The fact that the external field $\boldsymbol{g}_\mathrm{e}$ does not disappear from the internal dynamics can be interpreted as a violation of the strong version of the equivalence principle.[2] For the reader's convenience, we derive result (2) in Appendix A.

In a recent paper, Milgrom (2009) has shown that the imprint of the external galactic field, $\boldsymbol{g}_\mathrm{e}$, on the Solar system (due to violation of the strong equivalence principle) shows up not only asymptotically, but also in the inner regions of the system, where it may have implications for the motion of planets. This is somewhat unexpected because gravity is strong there (we have $g \gg a_0$) and the dynamics should be Newtonian. However, because of the special properties of equation (1), the solution will be given by some modified Poisson-type integral and the dynamics in the strong-field region will be affected by the anomalous behaviour in the asymptotic weak-field region. Thus, the results apply only to non-linear Poisson equation (1), not to modified inertia formulations of the MOND. The anomaly expresses itself as an anomalous quadrupolar contribution to the MONDian internal field u, as compared to the Newtonian potential, given by

$$\delta u = \frac{1}{2}x^i x^j Q_{ij}\,, \tag{3}$$

where x^i is the distance from the Solar system barycentre and Q_{ij} is a trace-free quadrupole moment of the type

$$Q_{ij} = Q_2\left(e^i e^j - \frac{1}{3}\delta_{ij}\right), \tag{4}$$

with Q_2 being the quadrupole coefficient and $\boldsymbol{e} = (e^i)$ is the preferred direction of the galactic centre (i.e. $\boldsymbol{e} = \boldsymbol{g}_\mathrm{e}/g_\mathrm{e}$). Anomalous term (3) is a harmonic solution of the Laplace equation, that is, $\Delta\delta u = 0$.

The radial dependence of this anomaly is $\propto r^2$ and can thus be separated from a quadrupolar deformation due to the Sun's oblateness which decreases like $\propto r^{-3}$. This result is valid whenever r is much less than the MOND transition distance for the Solar system, defined by $r_0 = \sqrt{GM/a_0}$ with M the mass of the Sun and a_0 the MOND acceleration scale. This radius corresponds to the transition region where the Newtonian acceleration becomes of the order of the MOND acceleration a_0 and therefore MOND effects become dominant. We have $r_0 \simeq 7100$ au, so effect (3) and (4) is valid in a large volume around the Sun, including all the planets (recall that Neptune's orbit is at 30 au).

In addition to effect (3), we also have the usual MOND effect. In the special case of spherical symmetry, equation (1) reduces to $\mu(g/a_0)g = g_\mathrm{N}$, with g_N the ordinary Newtonian gravitational field. For a MOND function behaving like $\mu(y) \sim 1 - \epsilon y^{-\gamma}$ when $y \to \infty$ (i.e. in the region $r \ll r_0$), the Newtonian field is modified by $\delta g_\mathrm{N} \simeq \epsilon a_0 (r/r_0)^{2\gamma-2}$. For $\gamma = 1$, this corresponds to a constant acceleration similar to the Pioneer anomaly and for $\gamma \geq 2$, the effect is very small and the motion of planets is almost unaffected. This effect is independent of the presence of the external field, and is spherical, so can be distinguished from quadrupolar deformation (3) induced by the external field; we neglect this effect here.

1.2 Summary

In this paper, we will confirm the existence of effect (3) and (4) and will derive it by an independent numerical integration of equation (1), using an elliptic solver originally built for numerical relativity purposes.[3] The magnitude of the quadrupole coefficient Q_2 depends on the dimensionless ratio between the external field g_e and the MOND acceleration a_0, say,

$$\eta = \frac{g_\mathrm{e}}{a_0}\,, \tag{5}$$

and on the particular MOND interpolating function μ in use. For the Milky Way field at the level of the Sun, we have $g_\mathrm{e} \simeq 1.9 \times 10^{-10}\,\mathrm{m\,s^{-2}}$, which happens to be slightly above the MOND scale, that is, $\eta \simeq 1.6$. Our calculation implemented for various standard choices for the μ-function gives

$$2.1 \times 10^{-27} \lesssim Q_2 \lesssim 4.1 \times 10^{-26}\ \mathrm{s^{-2}}\,. \tag{6}$$

[1] Recall that in the absence of the external field, the MOND potential behaves like $U \sim -\sqrt{GMa_0}\ln r$, showing that there is no escape velocity from an isolated system (Famaey, Bruneton & Zhao 2007). However, since no object is truly isolated, the asymptotic behaviour of the potential is always given by equation (2), in the approximation where the external field is constant.

[2] However, the weak version of the equivalence principle that all test particles in the MOND gravitational field have universal acceleration $\boldsymbol{a} = \boldsymbol{g}$ remains satisfied (Bekenstein & Milgrom 1984).

[3] The code is based on the library LORENE available from the website http://www.lorene.obspm.fr

The quadrupole coefficient Q_2 is found to be positive corresponding to a prolate elongation along the quadrupolar axis. We will verify numerically that Q_2 is indeed constant over a large portion of the inner Solar system and starts decreasing when the distance becomes comparable to the MOND transition scale r_0, at a few thousands au from the Sun. We will also check that Q_2 scales approximately like the inverse square root of the central mass, in agreement with dimensional analysis which shows that we should approximately have $Q_2 = q_2 a_0/r_0$, where $q_2(\eta)$ is a dimensionless quadrupole coefficient depending on the ratio η between the external field and the MOND acceleration. We find that for $\eta \simeq 1.6$, q_2 ranges over $0.02 \lesssim q_2 \lesssim 0.36$, in good agreement with the values found by Milgrom (2009).

We then study some consequences of the anomalous quadrupole moment for the motion of planets, notably the secular advances of planetary perihelia. Applying standard perturbation equations of celestial mechanics, we obtain the anomalous precession rate

$$\Delta_2 = \left\langle \frac{\mathrm{d}\tilde{\omega}}{\mathrm{d}t} \right\rangle = \frac{Q_2\sqrt{1-e^2}}{4n}\left[1 + 5\cos(2\tilde{\omega})\right]. \tag{7}$$

To simplify, we have assumed that the direction of the galactic centre lies in the plane of the ecliptic (this is only approximately correct) and that all planets move in this plane. We defined the origin of the precession angle $\tilde{\omega}$ to be the direction of the galactic centre. The orbital frequency of the planet is $n = 2\pi/P$ (P is the orbital period), and a, e and $\tilde{\omega} = \omega + \Omega$ denote the standard orbital elements. The effect seems to be the most interesting for Saturn for which we find

$$0.3 \lesssim \Delta_2 \lesssim 5.8\,\mathrm{mas\,cy^{-1}}. \tag{8}$$

Those values are within the range of published residuals for the precession of Saturn as obtained from global fits of the Solar system dynamics in Pitjeva (2005) and Fienga et al. (2009). However, we will find that in the case of the Earth, the predicted perihelion precession may be greatly constrained by the best estimates of post-fit residuals obtained, thanks to the Jupiter very long baseline interferometry (VLBI) data using the INPOP planetary ephemerides (Fienga et al. 2009). This is turn reduces the possible choices for the MOND function $\mu(y)$ to those that exhibit a sharp transition from the Newtonian to MONDian regime.

To conclude, we present very accurate numerical computations performed within well-defined theory (1) and compare the results with recent observations of the motion of planets in the Solar system. We find that the observational constraints are rather strong and may even conflict with some of the predictions. Thus, our results provide motivation for investigating more systematically possible anomalous effects in the Solar system, predicted by alternative theories. In particular, the EFE associated with the preferred direction of the galactic centre could be seen as a typical one arising in generic attempts to modify gravity with motivation coming from dark matter and/or dark energy. Indeed, we expect that generic departures from general relativity will violate the strong equivalence principle (Will 1993).

Conversely, let us cautiously remark that the MOND and more sophisticated theories, such as TeVeS (Bekenstein 2004), which are intended to describe the weak-field regime of gravity (below a_0), may not be extrapolated without modification to the strong field of the Solar system. For instance, it has been argued by Famaey & Binney (2005) that a MOND interpolating function μ which performs well at fitting the rotation curves of galaxies is given by μ_1 defined by equation (34a) below. However, this function has a rather slow transition to the Newtonian regime, given by $\mu_1 \sim 1 - y^{-1}$ when $y = g/a_0 \to \infty$, which is already excluded by Solar system observations (Sereno & Jetzer 2006). Indeed, such slow fall-off $-y^{-1}$ predicts a constant supplementary acceleration directed towards the Sun, $\delta g_\mathrm{N} = a_0$ (i.e. a 'Pioneer' effect), which is ruled out because it is not seen from the motion of planets. Thus, it could be that the transition between the MOND and Newtonian regimes is more complicated than is modelled in equation (1). This is also true for the modified dark matter model (Blanchet & Le Tiec 2008, 2009), which may only give an effective description valid in the weak-field limit and cannot be extrapolated as it stands to the Solar system. While looking at MOND-like effects in the Solar system, we should keep the previous *proviso* in mind. The potential conflict we find here with the Solar system dynamics (notably with the Earth orbital precession) may not necessarily invalidate those theories if they are not 'fundamental' theories but rather 'phenomenological' models.

The layout of this paper is as follows. In Section 2, we derive an expression of the solution of the MOND equation near the origin in terms of multipole moments. Section 3 is devoted to numerical techniques and results, with a description of the particular formulation and assumptions used for the numerical integration in Section 3.1, of the various tests passed by the code (Section 3.2), and the numerical results and values for the first multipoles of the potential are given in Section 3.3. Section 4 details the consequences of this modified gravitational potential on the orbits of Solar system planets, with first the derivation of the perturbation equations in Section 4.1 and numerical values for the planetary precessions (Section 4.2). Finally, Section 5 summarizes the results and gives some concluding remarks.

2 MULTIPOLAR EXPANSION OF THE MONDIAN POTENTIAL

In this paper, we will solve modified Poisson equation (1) with the boundary condition given by the constant external gravitational field $\boldsymbol{g}_\mathrm{e}$ (defining a preferred spatial direction denoted by $\boldsymbol{e} = \boldsymbol{g}_\mathrm{e}/g_\mathrm{e}$), that is, the gravitational field $\boldsymbol{g} = \nabla U$ asymptotes to $\lim_{r\to\infty} \boldsymbol{g} = \boldsymbol{g}_\mathrm{e}$. The external field $\boldsymbol{g}_\mathrm{e}$ should consistently obey a MOND equation, but here we will simply need to assume that $\boldsymbol{g}_\mathrm{e}$ is constant over the entire Solar system. The MONDian physicist measures from the motion of planets relative to the Sun the internal gravitational potential u defined by

$$u = U - \boldsymbol{g}_\mathrm{e}\cdot\boldsymbol{x}, \tag{9}$$

which is such that $\lim_{r\to\infty} u = 0$. Contrary to what happens in the Newtonian case, the external field $\boldsymbol{g}_\mathrm{e}$ does not disappear from gravitational field equation (1) and we want to investigate numerically its effect. The anomaly detected by a Newtonian physicist with respect to the MONDian physicist is the difference of internal potentials,

$$\delta u = u - u_\mathrm{N}, \tag{10}$$

where u_N denotes the ordinary Newtonian potential generated by the same ordinary matter distribution ρ and thus the solution of the Poisson equation $\Delta u_\mathrm{N} = -4\pi G\rho$ with the boundary condition that $\lim_{r\to\infty} u_\mathrm{N} = 0$. Hence, u_N is given by the standard Poisson integral

$$u_\mathrm{N}(\boldsymbol{x}, t) = G\int \frac{\mathrm{d}^3\boldsymbol{x}'}{|\boldsymbol{x}-\boldsymbol{x}'|}\,\rho(\boldsymbol{x}', t). \tag{11}$$

A short calculation shows that the anomaly obeys the ordinary Poisson equation $\Delta\delta u = -4\pi G\rho_\mathrm{pdm}$, where ρ_pdm is the density of 'phantom dark matter' defined by

$$\rho_\mathrm{pdm} = \frac{1}{4\pi G}\nabla\cdot(\chi\nabla U), \tag{12}$$

where we denote $\chi \equiv \mu - 1$. The phantom dark matter represents the mass density that a Newtonian physicist would attribute to dark matter. In the model by Blanchet & Le Tiec (2008, 2009), the phantom dark matter is interpreted as the density of polarization of some dipolar dark matter medium and the coefficient χ represents the 'gravitational susceptibility' of this dark matter medium.

The Poisson equation $\Delta\delta u = -4\pi G\rho_{\rm pdm}$ is to be solved with the boundary condition that $\lim_{r\to\infty}\delta u = 0$; hence, the solution is given by the Poisson integral

$$\delta u(\boldsymbol{x}, t) = G\int \frac{\mathrm{d}^3\boldsymbol{x}'}{|\boldsymbol{x}-\boldsymbol{x}'|}\,\rho_{\rm pdm}(\boldsymbol{x}', t)\,. \tag{13}$$

We emphasize here that, contrary to the Newtonian (linear) case, the knowledge of the matter density distribution does not allow to obtain any analytic solution for the potential; however, we can still infer the structure of the multipolar expansion near the origin and the moments will be computed numerically. We can check that the phantom dark matter behaves like r^{-3} when $r \to \infty$, so integral (13) is perfectly convergent.

We want to discuss the influence of the external galactic field in the inner part of the Solar system where the gravitational field is strong ($g \gg a_0$); thus, μ tends to 1 there, so χ tends to zero. For the discussion in this section, we adopt the extreme case where χ is *exactly* zero in a neighbourhood of the origin, say, for $r \leq \varepsilon$, so that there is no phantom dark matter for $r \leq \varepsilon$; in later sections devoted to the full numerical integration, we will still make this assumption by posing $\chi = 0$ inside the Sun (in particular, we will always neglect the small MOND effect at the centre of the Sun where gravity is vanishingly small). If $\rho_{\rm pdm} = 0$ when $r \leq \varepsilon$, we can directly obtain the multipolar expansion of anomalous term (13) about the origin by Taylor-expanding the integrand when $r = |\boldsymbol{x}| \to 0$. In this way, we obtain

$$\delta u = \sum_{l=0}^{+\infty} \frac{(-)^l}{l!}\,x^L Q_L\,, \tag{14}$$

where the multipole moments near the origin are given by[4]

$$Q_L = G\int_{r>\varepsilon} \mathrm{d}^3\boldsymbol{x}\;\rho_{\rm pdm}\,\partial_L\left(\frac{1}{r}\right). \tag{15}$$

Because the integration in equation (15) is limited to the domain $r > \varepsilon$ and $\partial_L(1/r)$ is STF there [indeed $\Delta(1/r) = 0$], we deduce that the multipole moments Q_L themselves are STF. This can also be immediately inferred from the fact that $\Delta\delta u = 0$ when $r \leq \varepsilon$; hence, multipole expansion (14) must be a homogeneous solution of the Laplace equation which is regular at the origin and is therefore necessarily made solely of STF tensors of type $\hat{x}^L$. Hence, we can replace x^L in equation (14) by its STF projection $\hat{x}^L$. It is clear from formula (15) that the MONDian gravitational field (for $r \geq r_0$) can influence the near-zone expansion of the field when $r \to 0$.

With expression (12) for the phantom dark matter and MOND equation (1), we can further transform Q_L as

$$Q_L = -\frac{1}{4\pi}\int_{r>\varepsilon} \mathrm{d}^3\boldsymbol{x}[4\pi G\rho + \Delta U]\partial_L\left(\frac{1}{r}\right). \tag{16}$$

[4] Our notation is as follows: $L = i_1 \ldots i_l$ denotes a multi-index composed of l multipolar spatial indices $i_1, \ldots, i_l$ (ranging from 1 to 3); $\partial_L = \partial_{i_1}\cdots\partial_{i_l}$ is the product of l partial derivatives $\partial_i \equiv \partial/\partial x^i$; $x^L = x^{i_1}\cdots x^{i_l}$ is the product of l spatial positions x^i; similarly, $n^L = n^{i_1}\cdots n^{i_l} = x^L/r^l$ is the product of l unit vectors $n^i = x^i/r$; the symmetric-trace-free (STF) projection is indicated with a hat, for instance, $\hat{x}^L \equiv \mathrm{STF}[x^L]$, and similarly for $\hat{n}^L$ and $\hat{\partial}_L$. The decomposition of ∂_L in terms of STF components $\hat{\partial}_L$ is given by equations (B2)–(B3) below. In the case of summed-up (dummy) multi-indices L, we do not write the l summations from 1 to 3 over their indices.

Approximating the central matter distribution as being spherically symmetric (i.e. ignoring the 'back-reaction' of the non-spherical anomalous field δu on the matter which generates the field), we see that the first term is non-zero only in the monopolar case $l = 0$ where it reduces in the limit $\varepsilon \to 0$ to minus the Newtonian potential evaluated at the origin. Conversely, the second term in equation (16) can be transformed as a surface integral. We find

$$Q_L = -u_{\rm N}(\boldsymbol{0})\delta_{l,0} + \frac{1}{4\pi}\int_{r=\varepsilon}^{r=\infty} \mathrm{d}^2 S_i\left[U\partial_{iL}\left(\frac{1}{r}\right) - \partial_i U\partial_L\left(\frac{1}{r}\right)\right]. \tag{17}$$

Our notation means that the surface integral is composed of two contributions, an inner one at $r = \varepsilon$ (denoted Q_L^ε) and an outer one at infinity $r = \infty$ (say Q_L^∞). In equation (17), we implicitly assume that the limit $\varepsilon \to 0$ is to be taken after evaluating the inner surface integral.

Inserting $U = u + \boldsymbol{g}_{\rm e}\cdot\boldsymbol{x}$ into the surface integral at infinity Q_L^∞, we find that it contributes only to the dipolar term and reduces to the external galactic field; thus, $Q_i^\infty = g_{\rm e}^i$ with all other values of Q_L^∞ being zero. Conversely, the inner surface integral Q_L^ε is found to have a well-defined limit when $\varepsilon \to 0$, given by $Q_L^\varepsilon = (-)^l(\hat{\partial}_L U)(\boldsymbol{0})$, where we recall that $\hat{\partial}_L$ denotes the STF part of $\partial_L = \partial_{i_1}\cdots\partial_{i_l}$. We then find that the galactic field in $U = u + \boldsymbol{g}_{\rm e}\cdot\boldsymbol{x}$ cancels the dipole term in the surface integral at infinity, so that the result is

$$Q_L = -u_{\rm N}(\boldsymbol{0})\delta_{l,0} + (-)^l(\hat{\partial}_L u)(\boldsymbol{0})\,. \tag{18}$$

The internal MONDian potential u admits therefore the following STF multipolar expansion (equivalent to a near-zone expansion when $r \to 0$):

$$u = u_{\rm N} - u_{\rm N}(\boldsymbol{0}) + \sum_{l=0}^{+\infty}\frac{1}{l!}x^L(\hat{\partial}_L u)(\boldsymbol{0})\,. \tag{19}$$

In Appendix B, we derive an alternative proof of this result. At this stage, we have elucidated the structure of the multipole expansion of the anomaly δu near the origin, but still we need to resort to a numerical integration of the non-linear MOND equation in order to obtain quantitative values for the multipole moments. Section 3 will be devoted to this task.

Finally, we show that the dipole moment Q_i (with $l = 1$) is actually zero (Milgrom 2009). This follows from the weak equivalence principle satisfied by the Bekenstein–Milgrom theory. As a consequence, the total acceleration of the centre of mass of the Solar system in the galactic external field $\boldsymbol{g}_{\rm e}$ does not depend on the Solar system's internal dynamics and is simply given by $\boldsymbol{g}_{\rm e}$ (for a detailed proof, see Bekenstein & Milgrom 1984). The centre of mass of the Solar system does not differ much from that of the Sun, so we deduce that the 'self-acceleration' of the Sun, that is, the total acceleration due to the internal potential u when integrated over the whole volume of the Sun, must be (approximately) zero:

$$\int \mathrm{d}^3\boldsymbol{x}\,\rho\partial_i u = 0\,. \tag{20}$$

We have obviously the same result for the Newtonian potential, $u_{\rm N}$, in Newtonian gravity, so the same will be true for the anomalous field $\delta u = u - u_{\rm N}$. In other words, the phantom dark matter, which is the source for the anomaly, exerts no net force on the Sun and we get, for a spherically symmetric star,

$$Q_i = -\frac{1}{M}\int \mathrm{d}^3\boldsymbol{x}\,\rho\partial_i\delta u = 0\,. \tag{21}$$

In Section 3.3, we will numerically verify that the dipole moment Q_i is indeed zero within our numerical error bars.

3 NUMERICAL INTEGRATION OF THE MOND EQUATION

3.1 Formulation and implementation

Using spherical spatial coordinates $\{r, \theta, \varphi\}$, we consider a star represented by a spherically symmetric distribution of matter $\rho(r)$ obtained from a hydrostatic equilibrium model in Newtonian theory (polytrope). These models are obtained by integrating the hydrostatic spherical equilibrium equation (relating the pressure p and the gravitational field) and the Newtonian equation for the gravitational field (relating the gravitational field and the density distribution ρ), together with a polytropic equation of state (EOS) of the form $p = K\rho^\gamma$, where K and γ are two constants. As it will be shown later in Section 3.2, the results do not depend on the specific EOS used to obtain this hydrostatic equilibrium, so we do not discuss the particular EOS used for obtaining the density distribution. It also means that we neglect the effect of MOND theory on the structure of the star. This is not a severe restriction, since inside the star, the gravitational field is much higher in amplitude than the constant a_0, making $\mu \sim 1$, and Newtonian theory is recovered up to very high accuracy. We then solve MOND equation (1), with the boundary conditions given by the constant galactic gravitational field $\boldsymbol{g}_\mathrm{e}$ (see Fig. 1), that is, $\lim_{r\to\infty} \boldsymbol{g} = \boldsymbol{g}_\mathrm{e} = g_\mathrm{e}\boldsymbol{e}$. In order to be closer to a Poisson-like form of the partial differential equation (PDE), we are solving in terms of the internal potential $u = U - \boldsymbol{g}_\mathrm{e}\cdot\boldsymbol{x}$, such that $\lim_{r\to\infty} u = 0$. Defining $\boldsymbol{h} = \nabla u = \boldsymbol{g} - \boldsymbol{g}_\mathrm{e}$, MOND equation (1) becomes the following PDE:

$$\Delta u = \frac{1}{\mu(g/a_0)}\left[-4\pi G\rho - \frac{\mu'(g/a_0)}{a_0 g}\, g^i g^j \partial_i h_j\right], \tag{22}$$

with $\mu' \equiv \mathrm{d}\mu/\mathrm{d}y$ being the derivative of the function μ with respect to its argument $y = g/a_0$.

This PDE is solved numerically, using the library LORENE, which implements spectral methods (for a review in the case of numerical relativity, see Grandclément & Novak 2009) in spherical coordinates. In our case (see Fig. 1), the fields do not depend on the azimuthal angle φ and the problem is axisymmetric. Since equation (22) is a non-linear elliptic PDE, the algorithm used is the fixed point iteration method in which one starts from an initial guess $u_0(r, \theta)$, here the solution of the Newtonian Poisson equation $\Delta u_0 = -4\pi G\rho$. Knowing $u_n(r, \theta)$ at a given iteration step n, one computes the non-linear source terms in the right-hand side of equation (22), say, $\sigma(u, \rho)$, to obtain a new value of the potential u_{n+1}, solving a linear Poisson equation

$$\Delta\tilde{u}_{n+1} = \sigma(u_n, \rho)\,, \tag{23}$$

and using a relaxation technique

$$u_{n+1} = \lambda\tilde{u}_{n+1} + (1-\lambda)u_n\,, \tag{24}$$

with $\lambda \in (0, 1]$ being the relaxation parameter (often taken to be 0.5). This iteration is stopped when the relative variation in the potential u between two successive steps becomes lower than a given threshold (usually 10^{-12}).

Linear equation (23) is solved by decomposing each field on a truncated base of spherical harmonics $Y_l^m(\theta, \varphi)$ (with $m = 0$, because the problem is axisymmetric) in the θ-direction and Chebyshev polynomials $T_n(r)$ in the r-direction. For the last coordinate, a multidomain technique is used, with linear mappings of the r-coordinate to the interval $[-1, 1]$, except for the last domain where a mapping of the type $s = 1/r$ allows to treat spatial infinity in our computational domain and to impose the right boundary conditions at $r \to \infty$ (see Grandclément & Novak 2009 for details). Moreover, this multidomain technique imposes that the potential u, as well as its first radial derivative, be continuous across the stellar surface.

Finally, the only modification made to the exact equation (22) in order to be numerically integrated is the setting $\mu(g/a_0) = 1$ inside the star. Indeed, there are two problems here. First, the MOND gravitational field $g(r)$ does not admit a regular Taylor expansion near the origin, as does the density in equation (B6) and the associated Newtonian gravitational field which follows as

$$g_\mathrm{N} = 4\pi G\sum_{k=0}^{+\infty}\frac{r^{2k+1}}{(2k+3)(2k+1)!}\,(\Delta^k\rho)(\mathbf{0})\,. \tag{25}$$

This can be immediately seen from the fact that in spherical symmetry, MOND equation (1) reduces to $\mu(g/a_0)g = g_\mathrm{N}$. Using equation (25), we see that the expansion of g when $r \to 0$ starts with a term proportional to the square root of r and is therefore not regular; more precisely, we have

$$g = \sqrt{\frac{4\pi G\rho_0 a_0 r}{3}}\left[1 + \mathcal{O}(r^2)\right]\,. \tag{26}$$

With our polynomial decomposition of fields in the radial direction, where we decompose in Chebyshev polynomials $T_n(r)$, we therefore get an incompatibility when trying to solve Poisson equation (23) in the vicinity of the origin at the centre of the Sun. The second problem is that, at the very centre of the star, $g \to 0$ and therefore $\mu \to 0$, which makes the division present in the right-hand side of equation (22) difficult to handle numerically.

Here, we have chosen to avoid both problems by imposing $\mu = 1$ in the star so it is entirely Newtonian. This approximation may produce a notable change in the value of $\mu(y)$ only within a sphere of radius $r \lesssim \frac{3a_0}{4\pi G\rho_0} \sim 10^{-15}\,\mathrm{R}_\odot$, where ρ_0 is the central density and $\mathrm{R}_\odot$ is the radius of the Sun. It is thus supposed to have a completely negligible effect on the results.

The result which is finally used to study the influence of the modification of the Newtonian gravity on the orbits of planets is the value of the trace-free multipole moments Q_L defined in Section 2. In the case where all the multipole moments are induced by the presence of the external field $\boldsymbol{g}_\mathrm{e}$ in the preferred direction $\boldsymbol{e}$, the situation is axisymmetric and all the moments Q_L will have their axis pointing in that direction $\boldsymbol{e}$ and we can define the multipole coefficients Q_l by

$$Q_L = Q_l\,\hat{e}^L\,, \tag{27}$$

where $\hat{e}^L$ denotes the STF part of the product of the l unit vectors $e^L = e^{i_1}\cdots e^{i_l}$. Then, multipole expansion (14) reads[5]

$$\delta u(r,\theta) = \sum_{l=0}^{+\infty}\frac{(-)^l}{(2l-1)!!}\,r^l\,Q_l(r)\,P_l(\cos\theta)\,, \tag{28}$$

where P_l is the usual Legendre polynomial and θ is defined in Fig. 1. Although from the considerations of Section 2 the multipole moments Q_l should be approximately constant within the MOND transition radius r_0, here, we compute them directly from the numerical solution of equation (1) and will obtain their dependence on r; we will check numerically that $Q_2(r)$ and $Q_3(r)$ are indeed almost constant in a large sphere surrounding the Solar system. With

[5] Here, the expansion is defined for any range in radius r, contrary to Section 2 and Appendix B, where the multipoles were only numbers defined for $r \to 0$ and not functions of r.

our definition, the monopole, quadrupole and octupole pieces in the internal field are, respectively, given by

$$\delta u_1 = -r\, Q_1\, \cos\theta, \tag{29a}$$

$$\delta u_2 = \frac{1}{2}\, r^2\, Q_2 \left(\cos^2\theta - \frac{1}{3}\right) \quad \text{and} \tag{29b}$$

$$\delta u_3 = -\frac{1}{6}\, r^3\, Q_3\, \cos\theta \left(\cos^3\theta - \frac{3}{5}\cos\theta\right), \tag{29c}$$

respectively. From dimensional arguments, it is possible to see that Q_l should scale as $Q_l \sim a_0/r_0^{l-1}$ (see, for instance, equations 33 and 37) and therefore[6]

$$\delta u \sim \sum_l Q_l r^l \sim a_0 r_0 \sum_l \left(\frac{r}{r_0}\right)^l. \tag{30}$$

The last expression shows that higher order multipoles should have lower influence on Solar system planets, for which $r \ll r_0$. This will be exemplified with the influence of the octupole, as compared to that of the quadrupole, in Section 4.2.

3.2 Tests of the code

A first test of our code is the standard comparison between the Laplace operator applied to the potential u and the right-hand side of equation (22). In all results displayed here, the maximum of this error has always remained lower than 10^{-11} and will not be considered as an interesting error indicator. Next, an indication of the error comes from the use of the Gauss theorem:

$$\oint \mu\left(\frac{g}{a_0}\right) \boldsymbol{g}\cdot \mathrm{d}^2\boldsymbol{S} = -4\pi G M, \tag{31}$$

where M is the mass of the star, computed from initial data at a very high precision. Then, another check (which is, however, not a priori independent) is the asymptotic behaviour of the potential $u(r, \theta)$ when $r \to \infty$, which is

$$u = \frac{GM}{r\mu_\mathrm{e}\sqrt{1+\lambda_\mathrm{e}\sin^2\theta}} + \mathcal{O}\left(\frac{1}{r^2}\right), \tag{32}$$

where $\mu_\mathrm{e} = \mu(y_\mathrm{e})$ and $\lambda_\mathrm{e} = y_\mathrm{e}\mu'_\mathrm{e}/\mu_\mathrm{e}$ with $y_\mathrm{e} = g_\mathrm{e}/a_0$ (see the proof in Appendix A). The two tests are not really independent, because the Gauss theorem is obtained by integrating the asymptotic field over a sphere at infinity. The main interest of these tests is that while the field is computed asymptotically on a sphere at infinity, the mass M is obtained 'locally' by integrating numerically the density over the volume of the star. We emphasize that in our code correct asymptotic behaviour (32) comes out directly and need not to be imposed by hands at the beginning of the calculation.

From the use of the mapping $s = 1/r$ (see Section 3.1), it is numerically possible to check the angular dependence of the quantity $r \times u$ when $r \to \infty$ and thus to estimate independently the error on the potential u. Both tests – Gauss theorem (31) and asymptotic behaviour (32) – have been performed and have given accuracy levels of $\sim 10^{-3}$–10^{-4}. Some examples are given in Fig. 2, for a sequence of different values for the asymptotic gravitational field g_e. Both tests give the same numbers, up to five digits. In all results shown hereafter, the accuracy level defined by these two tests is better than 10^{-2}.

[6] The radial dependence of the contribution of the lth multipole moment is the same as that of the usual MOND spherical effect corresponding to a MOND function behaving like $\mu \sim 1 - \epsilon y^{-\gamma}$ when $y \to \infty$, with $\gamma = (l+1)/2$ (see the discussion at the end of Section 1.1). But, of course, the effect we are considering here is non-spherical.

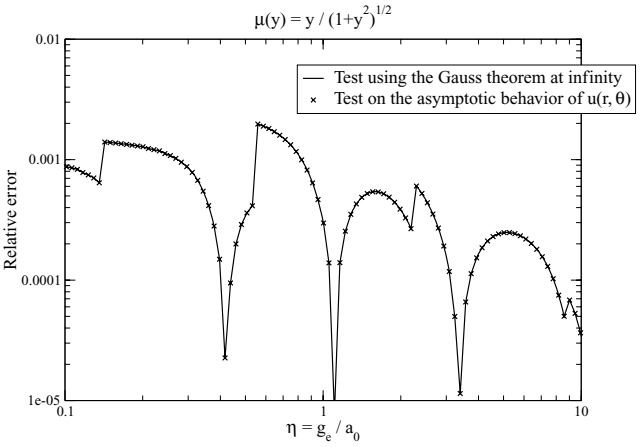

Figure 2. Relative error of the code on the two tests described in Section 3.2, for a 1-$\mathrm{M}_\odot$ spherical mass distribution, for the standard MOND function $\mu_2(y)$ (equation 34b) and the standard value $a_0 = 1.2 \times 10^{-10}\,\mathrm{m\,s^{-2}}$. The abscissa gives ratio (5) between the norm of the asymptotic gravitational field g_e and the parameter a_0. Note that both curves do coincide.

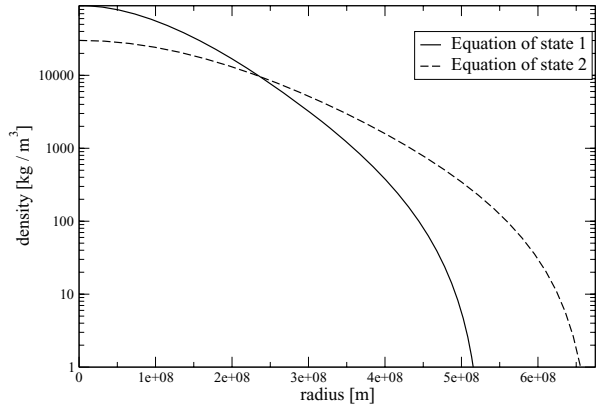

Figure 3. Two density profiles for testing the result dependence on the EOS. Both profiles yield a 1-$\mathrm{M}_\odot$ star in hydrostatic equilibrium. The two profiles yield very little (same level as the overall numerical accuracy $\sim 10^{-3}$) difference on our results.

Among the parameters entering the numerical model, we have checked that the details of the density profile $\rho(r)$ do not contribute to the value of the quadrupole moment $Q_2(r)$. As an illustration, we give here the quadrupole obtained with two different density profiles, displayed in Fig. 3, both giving a star of exactly $1\,\mathrm{M}_\odot$. With the same other parameters [choices of $\mu(y)$, a_0 and g_e], the relative difference in the induced quadrupole is 4×10^{-3}, while the error indicators give a relative numerical uncertainty of $\sim 2 \times 10^{-3}$. We therefore consider that the particular form of the density profile used to model the star (i.e. the choice of EOS) has little influence on the results.

3.3 Results on the induced quadrupole and octupole

In what follows, unless otherwise specified, the mass of the star is that of the Sun. As a first result, we show in Fig. 4 the profile of the quadrupole induced by the MOND theory through the function $Q_2(r)$ defined in equation (29b). We find that this quadrupole is decreasing from the star's neighbourhood to zero, on a typical

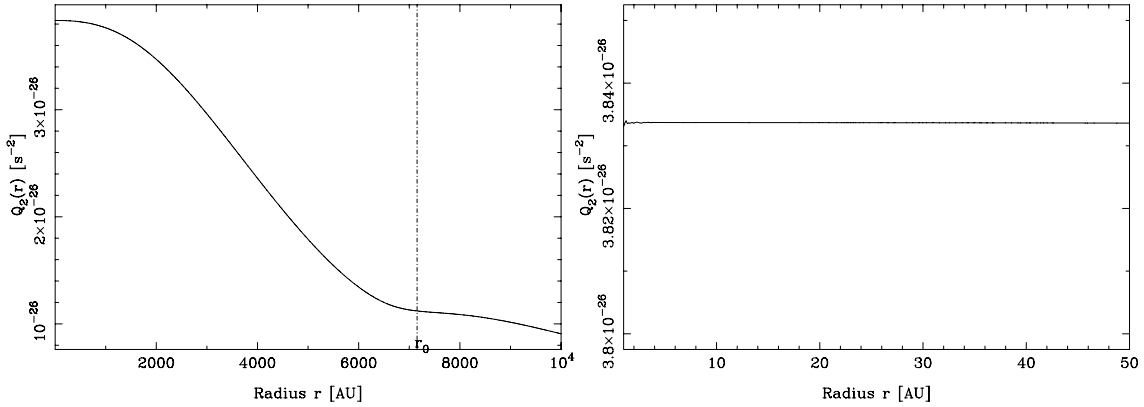

Figure 4. Left-hand panel: profile of $Q_2(r)$ in the Solar system for a standard choice of the function $\mu_1(y)$ (see equation 34a), $a_0 = 1.2 \times 10^{-10}\,\mathrm{m\,s^{-2}}$ and $g_\mathrm{e} = 1.9 \times 10^{-10}\,\mathrm{m\,s^{-2}}$. The MOND transition radius $r_0 = \sqrt{GM/a_0}$ is shown by a dot–dashed line at $r \simeq 7100$ au. Right-hand panel: zoom of the central region ($r \leq 50$ au), where the quadrupole is almost constant (the spikes for $r \to 0$ are due to the high value of the monopole term, from which it is numerically difficult to extract the quadrupole). Note the difference in the y-axis scales.

Table 1. Numerical values of the dipole Q_1, the quadrupole Q_2 and the octupole Q_3 together with the associated dimensionless quantities q_1, q_2 and q_3 defined by equations (33) and (37). All values are given near the Sun. We use different choices of the function $\mu(y)$ defined in equations (34) and (35). These values have been obtained for $a_0 = 1.2 \times 10^{-10}\,\mathrm{m\,s^{-2}}$ and $g_\mathrm{e} = 1.9 \times 10^{-10}\,\mathrm{m\,s^{-2}}$ (and $M = 1\,\mathrm{M}_\odot$).

MOND function	$\mu_1(y)$	$\mu_2(y)$	$\mu_5(y)$	$\mu_{20}(y)$	$\mu_\mathrm{exp}(y)$	$\mu_\mathrm{TeVeS}(y)$
Q_1 ($\mathrm{m\,s^{-2}}$)	-8.9×10^{-14}	-9.8×10^{-14}	-1.1×10^{-13}	-1.2×10^{-13}	-9.7×10^{-14}	-3.5×10^{-14}
q_1	-7.4×10^{-4}	-8.2×10^{-4}	-9.2×10^{-4}	-10^{-3}	-8.1×10^{-4}	-2.9×10^{-4}
Q_2 ($\mathrm{s^{-2}}$)	3.8×10^{-26}	2.2×10^{-26}	7.4×10^{-27}	2.1×10^{-27}	3.0×10^{-26}	4.1×10^{-26}
q_2	0.33	0.19	6.5×10^{-2}	1.8×10^{-2}	0.26	0.36
Q_3 ($\mathrm{m^{-1}\,s^{-2}}$)	-1.2×10^{-40}	-9.3×10^{-41}	-4.9×10^{-42}	-2.3×10^{-42}	-1.2×10^{-40}	-1.1×10^{-40}
q_3	-1.1	-0.87	-4.6×10^{-2}	-2.1×10^{-2}	-1.1	-1

scale of 10 000 au. However, this quadrupole can be considered as almost constant closer to the Sun, as it has a relative variation lower than 10^{-4} within 30 au (see the zoomed region in Fig. 4). We will therefore refer to the quadrupole as a simple number, noted $Q_2(0)$ or simply Q_2, when evaluating its influence on the orbits of Solar system planets. Our numerical results for the quadrupole are given in Table 1.

We now briefly study other multipole moments, namely, for $l = 1$ and 3. The profiles for the dipole $Q_1(r)$ and octupole $Q_3(r)$, defined by equations (29a) and (29c), are displayed in Fig. 5. We find that near the Sun and the solar planets, the dipole can be considered as zero, since it is three orders of magnitude lower than the typical value for an acceleration in the problem (i.e. a_0 or g_e). Indeed, we expect on dimensional analysis that Q_1 should scale with the MOND acceleration a_0 (see equation 30):

$$Q_1 = a_0\, q_1(\eta)\,, \tag{33}$$

where the dimensionless coefficient q_1 depends on the ratio η between g_e and a_0 as defined by equation (5). Our values given in Table 1 show that q_1 is actually very small. It means that Q_1 is lower than the numerical error and confirms the analytical proof given in Section 2 that the dipole moment is approximately zero.

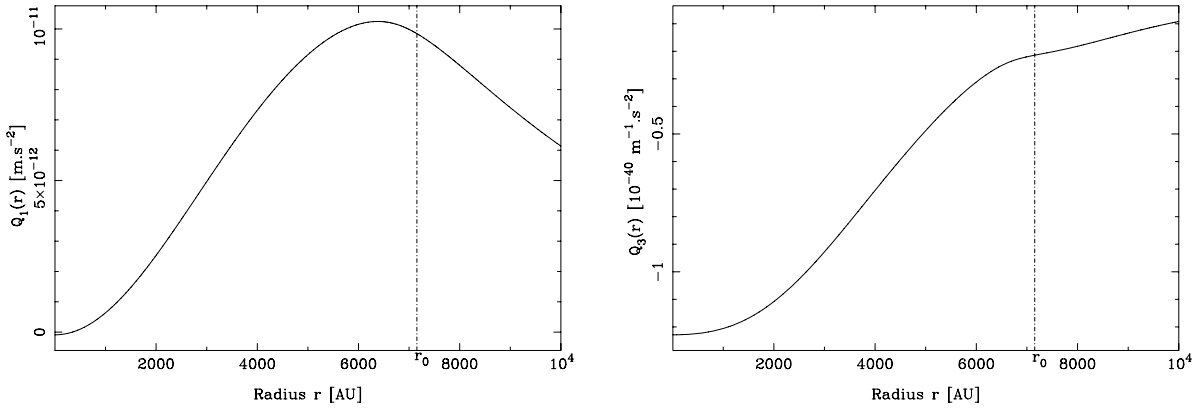

Figure 5. Profiles of the dipole $Q_1(r)$ (left-hand panel) and octupole $Q_3(r)$ (right-hand panel) in the Solar system, with the same settings as those of Fig. 4. The MOND transition radius $r_0 = \sqrt{GM/a_0}$ is shown by a dot–dashed line at $r \simeq 7100$ au. Numerically, we get $|Q_1(0)| \sim 9 \times 10^{-14}\,\mathrm{m\,s^{-2}} \ll a_0$ which shows that the dipole is in fact zero.

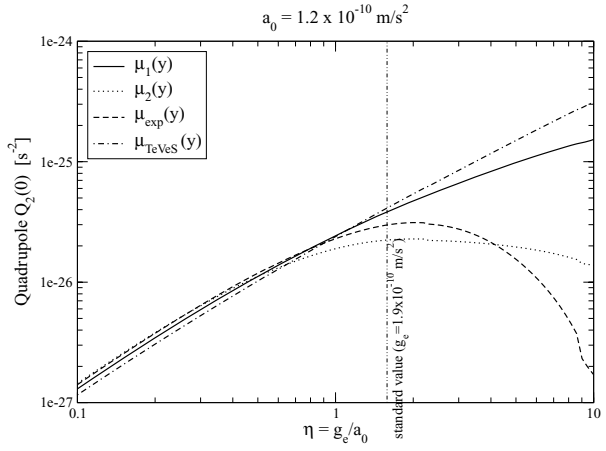

Figure 6. Quadrupole in the Solar system $Q_2 \equiv Q_2(0)$ as a function of the external galactic gravitational field g_e, for four different expressions of the coupling function $\mu(y)$ (see equations 34 for a description). The standard value of $g_e = 1.9 \times 10^{-10}\,\mathrm{m\,s^{-2}}$ is shown by a thin dash–double-dotted line.

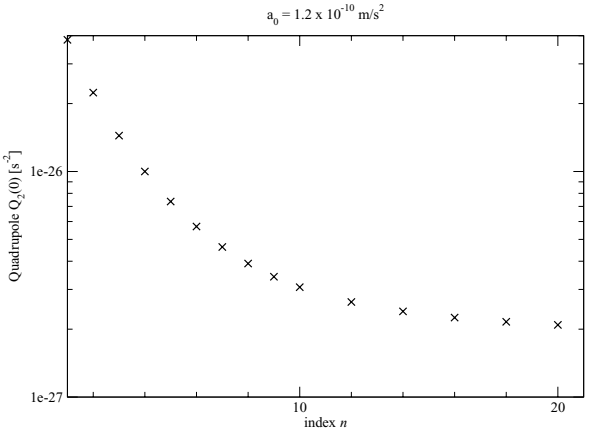

Figure 7. Quadrupole moment Q_2 as a function of the index n of the MOND function $\mu_n(y)$ defined by equation (35).

Conversely, we find that the octupole tends to a non-zero value, because the corresponding q_3, which has also an influence on the orbits of planets (see the next section), is found to be of the order of one. Numerical values of the octupole are also given in Table 1.

The dependence of the quadrupole moment Q_2 upon the value of the galactic gravitational field is displayed in Fig. 6, for four different coupling functions $\mu(y)$. Here, we consider four cases widely used in the literature:

$$\mu_1(y) = \frac{y}{1+y}\,, \tag{34a}$$

$$\mu_2(y) = \frac{y}{\sqrt{1+y^2}}\,, \tag{34b}$$

$$\mu_{\rm exp}(y) = 1 - \mathrm{e}^{-y}\,, \tag{34c}$$

$$\mu_{\rm TeVeS}(y) = \frac{\sqrt{1+4y}-1}{\sqrt{1+4y}+1}\,. \tag{34d}$$

The function μ_1 has been shown to yield good fits of galactic rotation curves (Famaey & Binney 2005). However, because of its slow transition to the Newtonian regime, it is a priori incompatible with Solar system observations. The function μ_2 is generally called the 'standard' choice and was used in fits such as those of Begeman, Broeils & Sanders (1991). We here use the general notation for any positive integer n:

$$\mu_n(y) = \frac{y}{\sqrt[n]{1+y^n}}. \tag{35}$$

We include also the function $\mu_{\rm exp}$ having an exponentially fast transition to the Newtonian regime. The fourth choice $\mu_{\rm TeVeS}$ is motivated by the theory TeVeS (Bekenstein 2004). One should note that none of these functions, except maybe the fourth one, derives from a fundamental physical principle.

One observes that, up to the standard value of $g_e = 1.9 \times 10^{-10}\,\mathrm{m\,s^{-2}}$, the four curves are quite close, giving an interval of values for Q_2:

$$2.2 \times 10^{-26} \lesssim Q_2 \lesssim 4.1 \times 10^{-26}\,\mathrm{s^{-2}}. \tag{36}$$

However, for other choices of the MOND function $\mu(y)$, Q_2 can take lower values down to $2.1 \times 10^{-27}\,\mathrm{s^{-2}}$. In all cases, we find that Q_2 is positive, which means a prolate deformation of the field towards the galactic centre. Two profiles of $\mu(y)$ seem to give a maximum for Q_2 near the standard value of g_e, namely, the standard choice μ_2 and the exponential choice $\mu_{\rm exp}$. For the two other choices of $\mu(y)$, we have not been able to increase the value of $\eta = g_e/a_0$ further than 10, because the error indicators would become too large and the results could not be trusted any longer. Note that in Fig. 6, a_0 has been kept fixed, while we have varied g_e. We have further explored the dependence of the EFE-induced quadrupole Q_2 on the type of MOND function.

We have used several different functions of type μ_n, as defined in equation (35), and the results for the variation in Q_2 depending on n are displayed in Fig. 7. From this figure, one can note that the value of Q_2 decreases with n, that is, with a faster transition from the weak-field regime [where $\mu(y) \sim y$] to the strong field regime [$\mu(y) \sim 1$]. We have been unable to study higher values of n and to determine a possible limit for Q_2 as n goes to infinity. In Table 1, we give values of the dipole, quadrupole and octupole near the Sun ($r \leq 50$ au), where they are observed to be constant, for four different expressions (34) of the interpolating function.

We have also explored different values of a_0 at fixed g_e, with the results that Q_2 was increasing for small a_0 as a power law, reaching a maximum value for $a_0 \simeq 10^{-10}$–$10^{-9}\,\mathrm{m\,s^{-2}}$ and then slowly decreasing. Finally, we have varied the mass of the central star. Results are displayed in Fig. 8 where, in particular, the $M^{-1/2}$ dependence of the quadrupole moment is recovered. This is not a surprise, since, on general grounds, one expects that the quadrupole moment (and similarly the octupole moment) should scale like (Milgrom 2009)[7]:

$$Q_2 = \frac{a_0}{r_0}\, q_2(\eta)\,, \tag{37a}$$

$$Q_3 = \frac{a_0}{r_0^2}\, q_3(\eta)\,, \tag{37b}$$

where $r_0 = \sqrt{GM/a_0}$ is the MOND transition radius, and q_2 and q_3 denote some dimensionless coefficients depending on the ratio $\eta = g_e/a_0$ and on the choice of the interpolating function μ. Having obtained the expected dependence on the mass in Fig. 8 is another

[7] To compare with the results of Milgrom (2009) for the quadrupole, one should note the different conventions in use, namely, $q_{ij}^{\rm Milgrom} = -Q_{ij}^{\rm BN}$ and $q^{\rm Milgrom}(\eta) = -\frac{2}{3} q_2^{\rm BN}(\eta)$. Our results for the quadrupole are in good agreement with values given by Milgrom (2009).

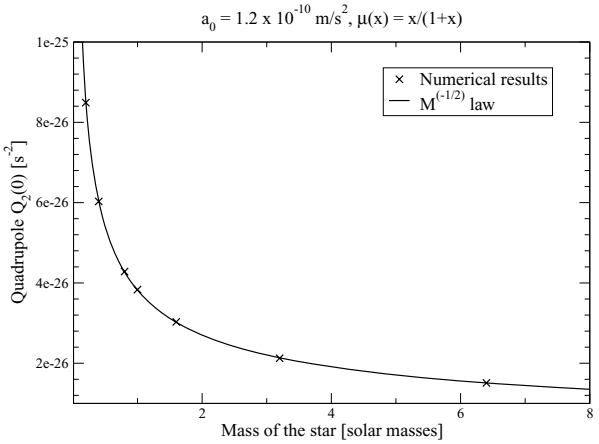

Figure 8. Quadrupole moment Q_2 as a function of the stellar mass M. The $M^{-1/2}$-law is recovered as expected from equation (37a).

check that our code behaves correctly, since we are able to recover the analytic results known for this system. The values of the dimensionless multipole coefficients q_2 and q_3, which are expectedly close to unity, are reported in Table 1.

4 EFFECT ON THE DYNAMICS OF SOLAR SYSTEM PLANETS

4.1 Perturbation equations

In this section, we investigate the consequence for the dynamics of inner planets of the Solar system of the presence of an abnormal multipole moment Q_L oriented towards the direction $\boldsymbol{e}$ of the galactic centre, in the sense of equation (27). Recall that the domain of validity of this anomaly is expected to enclose all the inner Solar system (for distances $r \lesssim r_0 \approx 7100$ au), with the quadrupole coefficient being constant up to, say, 50 au (see Fig. 4). As we have seen, the anomaly induces a perturbation on the Newtonian gravitational potential, namely, $u = u_{\rm N} + \delta u$, where the perturbation function δu is given for various multipole moments by equations (29). Following the standard practice of celestial mechanics, we denote the perturbation by $R \equiv \delta u$. The perturbation function R is such that the perturbing force (or, rather, acceleration) acting on the Newtonian motion is $\boldsymbol{F} = \nabla R$.

The unperturbed Keplerian orbit of a planet around the Sun is described by six orbital elements (say, c_A with $A = 1, \ldots, 6$). For these, we adopt the semimajor axis a, the eccentricity e, the inclination I of the orbital plane, the mean anomaly ℓ defined by $\ell = n(t - T)$, where $n = 2\pi/P$ (n is the mean motion, P is the orbital period and T is the instant of passage at the perihelion), the argument of the perihelion ω (or angular distance from ascending node to perihelion) and the longitude of the ascending node Ω. We also use the longitude of the perihelion defined by $\tilde{\omega} = \omega + \Omega$.

The perturbation is a function $R(c_A)$ of the orbital elements of the unperturbed Keplerian ellipse. With our choice for the orbital elements $\{c_A\} = \{a, e, I, \ell, \omega, \Omega\}$, the perturbation equations of celestial mechanics read (see e.g. Brouwer & Clemence 1961):

$$\frac{{\rm d}a}{{\rm d}t} = \frac{2}{an}\frac{\partial R}{\partial \ell}\,, \tag{38a}$$

$$\frac{{\rm d}e}{{\rm d}t} = \frac{\sqrt{1-e^2}}{ea^2n}\left[\sqrt{1-e^2}\frac{\partial R}{\partial \ell} - \frac{\partial R}{\partial \omega}\right], \tag{38b}$$

$$\frac{{\rm d}I}{{\rm d}t} = \frac{1}{a^2n\sqrt{1-e^2}\sin I}\left[\cos I\frac{\partial R}{\partial \omega} - \frac{\partial R}{\partial \Omega}\right], \tag{38c}$$

$$\frac{{\rm d}\ell}{{\rm d}t} = n - \frac{1}{a^2n}\left[2a\frac{\partial R}{\partial a} + \frac{1-e^2}{e}\frac{\partial R}{\partial e}\right], \tag{38d}$$

$$\frac{{\rm d}\omega}{{\rm d}t} = \frac{1}{a^2n}\left[\frac{\sqrt{1-e^2}}{e}\frac{\partial R}{\partial e} - \frac{\cos I}{\sin I\sqrt{1-e^2}}\frac{\partial R}{\partial I}\right], \tag{38e}$$

$$\frac{{\rm d}\Omega}{{\rm d}t} = \frac{1}{a^2n\sin I\sqrt{1-e^2}}\frac{\partial R}{\partial I}\,. \tag{38f}$$

We will be interested only in secular effects, so we average these equations over one orbital period P; denoting the time average by brackets, we have

$$\left\langle \frac{\partial R}{\partial c_A} \right\rangle = \frac{1}{P}\int_0^P {\rm d}t\,\frac{\partial R}{\partial c_A} = \frac{1}{2\pi}\int_0^{2\pi} {\rm d}\ell\,\frac{\partial R}{\partial c_A}\,. \tag{39}$$

In particular, this implies that we will always have $\langle \partial R/\partial \ell \rangle = 0$; hence, perturbation equation (38a) gives $\langle {\rm d}a/{\rm d}t \rangle = 0$ (at first order in perturbation theory). Indeed, a perturbative force of the type $\boldsymbol{F} = \nabla R$ is conservative, so the energy of the orbit is conserved in average and there is no secular change in the semimajor axis.

Let us now apply perturbation equations (38) to the specific case of the perturbation function corresponding to the quadrupole anomaly, namely,

$$R = \delta u_2 = \frac{1}{2}r^2\,Q_2\left(\cos^2\theta - \frac{1}{3}\right). \tag{40}$$

Here $\cos\theta = \boldsymbol{e}\cdot\boldsymbol{n}$, with $\boldsymbol{n} = \boldsymbol{x}/r$ being the unit direction of the planet and $r^2 = x^2 + y^2 + z^2$, where (x, y, z) are the coordinates of the planet in an absolute Galilean frame centred on the focus of the unperturbed Keplerian ellipse and with respect to which the orbital elements $\{a, e, I, \ell, \omega, \Omega\}$ are defined. In the following, to simplify the presentation, we will choose the x-direction of this Galilean frame to be the direction of the galactic centre $\boldsymbol{e} = \boldsymbol{g}_{\rm e}/g_{\rm e}$. That is, we assume that the origin of the longitude of the ascending node Ω lies in the direction of the galactic centre. This means that $\cos\theta = x/r$, so that

$$R = \frac{Q_2}{6}\left(2x^2 - y^2 - z^2\right). \tag{41}$$

We express the planet's absolute coordinates (x, y, z) in terms of the orbital elements $\{a, e, I, \ell, \omega, \Omega\}$ by performing as usual three successive frame rotations with angles Ω, I and ω, to arrive at the frame (u, v, w) associated with the motion, where (u, v) is in the orbital plane, with u in the direction of the perihelion and v oriented in the sense of motion at perihelion. The unperturbed coordinates of the planet in this frame are

$$u = a\,(\cos U - e)\,, \tag{42a}$$

$$v = a\sqrt{1-e^2}\sin U\,, \tag{42b}$$

$$w = 0\,, \tag{42c}$$

where U denotes the eccentric anomaly, related to ℓ by the Kepler equation $\ell = U - e\sin U$. Inserting the resulting expression of R into perturbation equations (38) and performing the time-average (in practice, an average over the eccentric anomaly U, after the appropriate change in variable) yields

$$\left\langle \frac{{\rm d}a}{{\rm d}t} \right\rangle = 0\,, \tag{43a}$$

$$\left\langle \frac{\mathrm{d}e}{\mathrm{d}t} \right\rangle = \frac{5Q_2 e\sqrt{1-e^2}}{4n} \times \left[\cos I \cos(2\omega)\sin(2\Omega) + \sin(2\omega)(\cos^2\Omega - \cos^2 I \sin^2\Omega)\right] , \tag{43b}$$

$$\left\langle \frac{\mathrm{d}I}{\mathrm{d}t} \right\rangle = \frac{Q_2 \sin I \sin\Omega}{4n\sqrt{1-e^2}} \times \left\{ \left[2 + 3e^2 + 5e^2\cos(2\omega)\right]\cos\Omega - 5e^2 \cos I \sin(2\omega)\sin\Omega \right\} , \tag{43c}$$

$$\begin{aligned}\left\langle \frac{\mathrm{d}\ell}{\mathrm{d}t} \right\rangle = n + \frac{Q_2}{96n} \Big\{ & -15(1+e^2)\cos(2\omega)\left[2 - 2\cos(2I)\right. \\ & \left. + \cos(2I - 2\Omega) + 6\cos(2\Omega) + \cos(2I + 2\Omega)\right] \\ & + 12\left(-8 + 3e^2\right)\cos^2\Omega \\ & - 12\left[1 - 6e^2 + (7 + 3e^2)\cos(2I)\right]\sin^2\Omega \\ & + 20\left[2 - 3e^2 + 6(1+e^2)\cos I \sin(2\omega)\sin(2\Omega)\right] \Big\} ,\end{aligned} \tag{43d}$$

$$\begin{aligned}\left\langle \frac{\mathrm{d}\omega}{\mathrm{d}t} \right\rangle = & -\frac{Q_2}{4n\sqrt{1-e^2}} \\ & \times \Big\{ 2 - 2e^2 + (-1+e^2)\left[3 + 5\cos(2\omega)\right]\cos^2\Omega \\ & + \frac{5}{2}e^2 \cos I \sin(2\omega)\sin(2\Omega) - 10\cos^2 I \sin^2\omega \sin^2\Omega \\ & + 5(1-e^2)\cos I \sin(2\omega)\sin(2\Omega) \Big\} ,\end{aligned} \tag{43e}$$

$$\left\langle \frac{\mathrm{d}\Omega}{\mathrm{d}t} \right\rangle = \frac{Q_2 \sin\Omega}{4n\sqrt{1-e^2}} \times \left\{ 5e^2 \cos\Omega \sin(2\omega) + \cos I \left[-2 - 3e^2 + 5e^2\cos(2\omega)\right]\sin\Omega \right\} . \tag{43f}$$

These equations are general and give in particular the precession of the node $\langle \mathrm{d}\Omega/\mathrm{d}t \rangle$ and the perihelion precession $\langle \mathrm{d}\omega/\mathrm{d}t \rangle$ or, rather, $\langle \mathrm{d}\tilde{\omega}/\mathrm{d}t \rangle$, where $\tilde{\omega} = \omega + \Omega$ is the longitude of the perihelion.

In order to make some estimate of the magnitude of the effect, let us approximate the direction of the galactic centre (which is only 5.°5 off the plane of the ecliptic)[8] as being located in the plane of the orbit; consequently, we choose $I = 0$. In this case, $\tilde{\omega} = \omega + \Omega$ is the relevant angle for the argument of the perihelion. The non-zero evolution equations then become

$$\left\langle \frac{\mathrm{d}e}{\mathrm{d}t} \right\rangle = \frac{5Q_2 e\sqrt{1-e^2}}{4n} \sin(2\tilde{\omega}) , \tag{44a}$$

$$\left\langle \frac{\mathrm{d}\ell}{\mathrm{d}t} \right\rangle = n - \frac{Q_2}{12n}\left[7 + 3e^2 + 15(1+e^2)\cos(2\tilde{\omega})\right] , \tag{44b}$$

$$\left\langle \frac{\mathrm{d}\tilde{\omega}}{\mathrm{d}t} \right\rangle = \frac{Q_2\sqrt{1-e^2}}{4n}\left[1 + 5\cos(2\tilde{\omega})\right] . \tag{44c}$$

We recall that with our notation, $\tilde{\omega}$ is the azimuthal angle between the direction of the perihelion and that of the galactic centre (approximated to lie in the orbital plane). Of particular interest is the secular precession of the perihelion $\langle \mathrm{d}\tilde{\omega}/\mathrm{d}t \rangle$ due to the quadrupole effect which we henceforth denote by[9]

$$\Delta_2 = \frac{Q_2\sqrt{1-e^2}}{4n}\left[1 + 5\cos(2\tilde{\omega})\right] . \tag{45}$$

The precession is non-spherical in the sense that it depends on the orientation of the orbit relative to the galactic centre through its dependence upon the perihelion's longitude $\tilde{\omega}$. The effect scales with the inverse of the orbital frequency, $n = 2\pi/P$, and therefore becomes more important for outer planets like Saturn than for inner planets like Mercury. This is in agreement with the fact that the quadrupole effect we are considering increases with the distance to the Sun (but of course will fall down when r becomes appreciably comparable to r_0, see Fig. 4).

We have also computed the secular planetary precession induced by the octupole moment Q_3, for which the perturbation function reads, with the same conventions,

$$\begin{aligned}R &= -\frac{1}{6}r^3 Q_3 \left(\cos^3\theta - \frac{3}{5}\cos\theta\right) \\ &= -\frac{Q_3}{30}x\left(2x^2 - 3y^2 - 3z^2\right) .\end{aligned} \tag{46}$$

Redoing the perturbation analysis, we find the octupolar precession in the case $I = 0$ as

$$\Delta_3 = \frac{Q_3 a\sqrt{1-e^2}}{32en}\left[2 - 13e^2 + 35e^2\cos(2\tilde{\omega})\right]\cos\tilde{\omega} . \tag{47}$$

4.2 Numerical evaluation of the planetary precession

We now compute numerically this effect for the various planets of the Solar system; the relevant orbital elements for the planets we used in this calculation are provided in Table 2.

Our numerical values for the quadrupole and octupole anomalies, Δ_2 and Δ_3, are reported in Tables 3 and 4, respectively. As we see from Table 3, the quadrupolar precession Δ_2 is in the range of milliarcsecond per century (mas cy^{-1}), which is not negligible. In particular, it becomes interestingly large for the outer gaseous planets of the Solar system, essentially Saturn, Uranus and Neptune. The dependence on the choice of the MOND function μ is notable only for functions $\mu_n(y)$ defined by equation (35) with large values of n, where the effect decreases by a factor of $\sim$10 between $n = 2$ and 20. However, the octupolar precession, Δ_3, in Table 4 is much smaller, being rather in the range of μas cy^{-1}.

We give for comparison in Table 5 the best-published post-fit residuals for any possible supplementary precession of planetary orbits (after the relativistic precession has been duly taken into account), which have been obtained from global fits of the Solar system dynamics by Pitjeva (2005) and Fienga et al. (2009). In particular, the INPOP planetary ephemerides by Fienga et al. (2009) use information from the combination of very accurate tracking data of spacecrafts orbiting different planets.

From Table 5, we see that our results for Δ_2 are smaller or much smaller than the published residuals except for the planets Earth, Mars and Saturn. The case of Saturn is interesting because the INPOP planetary ephemerides by Fienga et al. (2009) publish an offset with respect to the general relativistic value for the precession, namely, they quote -10 ± 8 mas cy^{-1} as obtained from the Cassini

[8] The latitude β and longitude λ of the galactic centre in the standard ecliptic coordinate system are $\beta = -5.°5$ and $\lambda = -93.°2$ (see e.g. Allen 1999).

[9] The result found by Milgrom (2009) for this effect (his equations 37 and 38) looks more complicated, but can be simplified and is seen to be equivalent to ours.

Table 2. Orbital elements of planets used in the computation of the abnormal precession rates Δ_2 and Δ_3. The longitude of the perihelion $\tilde{\omega}$ is defined here with respect to the direction of the external galactic field (assuming that the galactic centre lies within the plane of the ecliptic). Thus, we pose $\tilde{\omega} = \tilde{\omega}_{\rm Allen} - \lambda$, where $\lambda = -93.^\circ 2$ is the longitude of the galactic centre and $\tilde{\omega}_{\rm Allen}$ is given in Allen (1999).

	Mercury	Venus	Earth	Mars	Jupiter	Saturn	Uranus	Neptune
a (au)	0.397	0.723	1.00	1.523	5.203	9.537	19.229	30.069
e	0.206	0.007	0.017	0.093	0.048	0.054	0.047	0.009
P (yr)	0.24	0.62	1.00	1.88	11.86	29.46	84.01	164.8
$\tilde{\omega}$ ($^\circ$)	170.7	224.7	196.1	69.2	108.0	185.6	264.2	138.2

Table 3. Results for the precession rates of planets, Δ_2, due to the quadrupole coefficient Q_2. We use the values for Q_2 corresponding to various MOND functions defined in equations (34) and (35) (see Table 1). All results are given in mas cy^{-1}.

	Quadrupolar precession rate, Δ_2, in mas cy^{-1}							
MOND function	Mercury	Venus	Earth	Mars	Jupiter	Saturn	Uranus	Neptune
$\mu_1(y)$	0.04	0.02	0.16	−0.16	−1.12	5.39	−10.14	7.93
$\mu_2(y)$	0.02	0.01	0.09	−0.09	−0.65	3.12	−5.87	4.59
$\mu_5(y)$	7×10^{-3}	3×10^{-3}	0.03	−0.03	−0.22	1.05	−1.97	1.54
$\mu_{20}(y)$	2×10^{-3}	10^{-3}	9×10^{-3}	-9×10^{-3}	−0.06	0.3	−0.56	0.44
$\mu_{\rm exp}(y)$	0.03	0.02	0.13	−0.13	−0.88	4.25	−8.01	6.26
$\mu_{\rm TeVeS}(y)$	0.05	0.02	0.17	−0.17	−1.21	5.81	−10.94	8.56

Table 4. Results for the precession rates of planets, Δ_3, due to the octupole coefficient Q_3. The results are given in μas cy^{-1}.

	Octupolar precession rate, Δ_3, in μas cy^{-1}							
MOND function	Mercury	Venus	Earth	Mars	Jupiter	Saturn	Uranus	Neptune
$\mu_1(y)$	2×10^{-3}	0.2	0.2	−0.03	1.4	19.5	12.1	1499
$\mu_2(y)$	2×10^{-3}	0.1	0.2	−0.03	1.1	15.1	9.4	1162
$\mu_5(y)$	10^{-4}	5×10^{-3}	0.01	-2×10^{-3}	0.06	0.8	0.5	61.2
$\mu_{20}(y)$	5×10^{-5}	2×10^{-3}	5×10^{-3}	-7×10^{-4}	0.03	0.4	0.2	28.7
$\mu_{\rm exp}(y)$	2×10^{-3}	0.2	0.2	−0.03	1.4	19.5	12.1	1499
$\mu_{\rm TeVeS}(y)$	2×10^{-3}	0.2	0.2	−0.03	1.3	17.9	11.1	1374

Table 5. Reproduction of some published residuals for any supplementary orbital planetary precession. All results are given in mas cy^{-1}.

	Post-fit residuals for $\Delta = \langle {\rm d}\tilde{\omega}/{\rm d}t \rangle$ in mas cy^{-1}							
Origin	Mercury	Venus	Earth	Mars	Jupiter	Saturn	Uranus	Neptune
Pitjeva (2005)	-3.6 ± 5	-0.4 ± 0.5	-0.2 ± 0.4	0.1 ± 0.5	–	-6 ± 2	–	–
Fienga et al. (2009)	-10 ± 30	-4 ± 6	0 ± 0.016	0 ± 0.2	142 ± 156	-10 ± 8	$0 \pm 2 \times 10^4$	$0 \pm 2 \times 10^4$

tracking data and 200 ± 160 mas cy^{-1} from the VEX data. The values we find for Δ_2 are smaller but grossly within the range of these post-fit residuals. However, we find that Δ_2 is positive for Saturn, while the offset reported in Fienga et al. (2009) from Cassini data is negative. But note that this may not be relevant, because the INPOP ephemerides are used by Fienga et al. (2009) to detect the presence of an eventual abnormal precession, not to adjust the value of that precession.

In the case of the Earth, the INPOP ephemerides find a tight constraint 0 ± 0.016 coming from the Jupiter VLBI data (Fienga et al. 2009). This constraint seems already to exclude most of our obtained values for Δ_2, except for MOND functions of type μ_n (equation 35) with rather large values of n. In particular, one needs to take $n > 8$ in order to have an EFE precession compatible with this constraint on the Earth orbit. Conversely, we note that for all the planets, the octupolar precession rate, Δ_3, is very small and clearly completely negligible in current fits of the Solar system dynamics.

Thus, it seems that in the case of the Earth, the constraint from the Jupiter VLBI data is already quite tight and it is difficult to accommodate our anomalous quadrupolar precession rate, Δ_2, for most choices of the MOND function $\mu(y)$. However, let us remark that the post-fit residuals in Table 5 are obtained by adding by hands an excess of precession for the planets and looking for the tolerance of the data on this excess. But, in order to really test the anomalous quadrupolar precession rate, Δ_2, one should consistently work in a MOND picture, that is, one should also consider the other effects predicted by this theory, like the precession of the nodes, the variation in the eccentricity and the inclination. Then, one should perform a global fit of all these effects to the data; it is likely that in this way the quantitative conclusions would be different.

Conversely, as we have commented in the Introduction, it is non-trivial to know if testing MOND-like theories (including TeVeS and the model proposed by Blanchet & Le Tiec 2008, 2009) in the Solar system could invalidate those theories, if they represent only some phenomenological models describing the weak-field regime

of gravity and as such should not be extrapolated as they are in the strong field of the Solar system.

5 CONCLUSION

In MONDian gravity, the influence of the external galactic gravitational field on to the orbits of Solar system planets appears mainly through the presence of a quadrupolar perturbation to the gravitational potential, as it has been shown through a multipolar analysis of the solution of the MOND equation. This contribution has been computed using a spectral, highly accurate, numerical Poisson solver to obtain a solution of equation (1). This numerical solution has been extensively tested and compared to known analytical formulae and all the expected properties have been recovered. Using the most commonly used MOND coupling functions, $\mu(y)$, and value of the MOND acceleration, a_0, we have obtained quadrupole contributions that are compatible with those published by Milgrom (2009). We have also extended this calculation to include octupole contributions. With the derivation of detailed perturbation equations, the influence of the quadrupole and octupole on the perihelion precession of planets has been quantified and compared to two sets of observations, in particular, the INPOP planetary ephemerides by Fienga et al. (2009).

At first sight, these observational results seem to exclude the presence of a MOND-EFE-induced quadrupole, for some choices of the MOND function μ and scale a_0. This is particularly true for the Earth orbit, where constraints from the Jupiter VLBI observations are very strong. However, for other choices of the MOND function, the observational constraints on the precession of the Earth orbit are still compatible with the computed effect. These compatible MOND functions share the property of having a very sharp transition from the weak-field (modified) to the strong-field (Newtonian) regime. Moreover, one should be very cautious and keep in mind the following:

(1) The observational constraints on the Solar system orbits have been obtained by a global fit, using a fully relativistic first-post-Newtonian model. Taking into account only a particular MOND effect, like precession, without considering a fully-MONDian model is, in principle, incoherent, since all the other effects should also be considered.

(2) The MOND theory is a phenomenological approach trying to describe gravity in the weak-field regime (where evidence for dark matter arises). It is therefore unclear if such theory can be applied to stronger gravitational fields and, in particular, in the Solar system. Conversely, the constraints obtained here in strong field may not be relevant for the weak-field case, unless some more fundamental theory, valid in both regimes, is known.

In any case, further studies are to be done if one wants to obtain more stringent conclusions about constraints imposed by Solar system observations on to MOND-like theories. More precise observations could also provide valuable information about an eventual EFE due to MOND theory and also restrict the number of possible MOND functions that are compatible with the observations.

ACKNOWLEDGMENT

It is a pleasure to thank Christophe Le Poncin-Lafitte, Alexandre Le Tiec and Mordehai Milgrom for a careful reading of this manuscript and very useful comments.

REFERENCES

Allen C., 1999, Astrophysical Quantities. Springer-Verlag, Berlin
Begeman K., Broeils A., Sanders R., 1991, MNRAS, 249, 523
Bekenstein J., 2004, Phys. Rev. D, 70, 083509
Bekenstein J., 2005, in Domokos G., Kaplan D. E., Kovesi-Domokos S., Sundrum R., eds, Proc. 28th John Hopkins Workshop on Current Problems in Particle Theory, p. 012
Bekenstein J., Milgrom M., 1984, ApJ, 286, 7
Blanchet L., 2007, Class. Quantum Gravity, 24, 3529
Blanchet L., Damour T., 1986, Phil. Trans. R. Soc. A, 320, 379
Blanchet L., Le Tiec A., 2008, Phys. Rev. D, 78, 024031
Blanchet L., Le Tiec A., 2009, Phys. Rev. D, 80, 023524
Brouwer D., Clemence G. M., 1961, Methods of Celestial Mechanics. Academic Press, New York
Famaey B., Binney J., 2005, MNRAS, 363, 603
Famaey B., Bruneton J. P., Zhao H., 2007, MNRAS, 377, L79
Fienga A., Laskar J., Kuchynka P., Leponcin-Laffite C., Manche H., Gastineau M., 2009, in Klioner S., Seidelmann P. K., Soffel M., eds, Proc. IAU Symp. Vol. 261, Relativity in Fundamental Astronomy: Dynamics, Reference Frames and Data Analysis. Cambridge Univ. Press, Cambridge, p. 159
Granclément P., Novak J., 2009, Living Rev. Relat., 12, 1 (http://www.livingreviews.org/lrr-2009-1)
Milgrom M., 1983a, ApJ, 270, 365
Milgrom M., 1983b, ApJ, 270, 371
Milgrom M., 1983c, ApJ, 270, 384
Milgrom M., 2009, MNRAS, 399, 474
Pitjeva E., 2005, Astron. Lett., 31, 340
Sanders R., 2005, MNRAS, 363, 459
Sanders R., McGaugh S., 2002, ARA&A, 40, 262
Sereno M., Jetzer P., 2006, MNRAS, 371, 626
Will C. M., 1993, Theory and Experiment in Gravitational Physics. Cambridge Univ. Press, Cambridge

APPENDIX A: ASYMPTOTIC BEHAVIOUR OF THE FIELD

In this appendix, we prove that the asymptotic behaviour of the solution of Bekenstein–Milgrom equation (1) at large distances from an isolated matter source in the presence of an external field, $\boldsymbol{g}_\mathrm{e}$, is given by equation (32). The proof has already been given by Bekenstein & Milgrom (1984); here, we present a slightly different derivation. For simplicity, we suppose that the source is spherically symmetric, so that the asymptotic form of the MOND potential is axisymmetric around the direction of the external field and of the type

$$U = g_\mathrm{e}^i x^i + \frac{f(\theta)}{r} + \mathcal{O}\left(\frac{1}{r^2}\right) , \tag{A1}$$

where $f(\theta)$ is a function of the azimuthal angle θ measured from the direction $\boldsymbol{e}$ of the external field. We naturally assume that the function $f(\theta)$ is regular. With ansatz (A1), we obtain successively the leading order terms in the expansion of various quantities as

$$g^i = g_\mathrm{e}^i + \frac{1}{r^2}\left[\left(-f + \frac{\cos\theta}{\sin\theta} f_\theta\right) n^i - \frac{f_\theta}{\sin\theta} e^i\right] + \mathcal{O}\left(\frac{1}{r^3}\right) , \tag{A2a}$$

$$\mu = \mu_\mathrm{e}\left(1 + \frac{\lambda_\mathrm{e}}{g_\mathrm{e} r^2}\left[-\cos\theta f - \sin\theta f_\theta\right]\right) + \mathcal{O}\left(\frac{1}{r^3}\right) , \tag{A2b}$$

$$\mu g^i = \mu_\mathrm{e}\left(g_\mathrm{e}^i + \frac{1}{r^2}\left[\left(-\lambda_\mathrm{e} f\cos\theta - \lambda_\mathrm{e} f_\theta \sin\theta - \frac{f_\theta}{\sin\theta}\right) e^i + \left(-f + \frac{\cos\theta}{\sin\theta} f_\theta\right) n^i\right]\right) + \mathcal{O}\left(\frac{1}{r^3}\right) , \tag{A2c}$$

where we denote $f_\theta \equiv \partial f/\partial\theta$, $\mu_\mathrm{e} \equiv \mu(y_\mathrm{e})$, $\lambda_\mathrm{e} \equiv y_\mathrm{e}\mu'_\mathrm{e}/\mu_\mathrm{e}$ [with $y_\mathrm{e} = g_\mathrm{e}/a_0$ and $\mu'_\mathrm{e} = \mathrm{d}\mu\,(y_\mathrm{e})/\mathrm{d}y_\mathrm{e}$]. Next, we impose that $\partial_i(\mu g^i) = 0$ holds asymptotically far from a localized matter distribution. This, together with the fact that f is a regular function of the azimuthal angle θ, yields the first-order differential equation

$$\left(1 + \lambda_\mathrm{e}\sin^2\theta\right) f_\theta + \lambda_\mathrm{e}\sin\theta\cos\theta\, f = 0\,, \tag{A3}$$

whose solution is given in terms of a constant K by

$$f = \frac{K}{\sqrt{1 + \lambda_\mathrm{e}\sin^2\theta}}\,. \tag{A4}$$

Finally, we determine this constant by using Gauss theorem (31), that is,

$$\oint \mu g^i r^2 n^i \mathrm{d}\Omega = -4\pi G M, \tag{A5}$$

where we choose a coordinate sphere, since the result does not depend on the chosen surface at infinity. Inserting into equation (A5) the asymptotic expansion of the field given by equation (A2c), together with the solution (A4) found for f, we obtain

$$K = \frac{GM}{\mu_\mathrm{e}}\,, \tag{A6}$$

which establishes the looked-for formula (equation 32).

APPENDIX B: EXPRESSION OF THE MULTIPOLE EXPANSION

Result (19) can also be proved directly, without resorting to the computation of surface integrals of Section 2. We first expand $\delta u = u - u_\mathrm{N}$, when $r \to 0$, using Taylor's formula as

$$\delta u = \sum_{l=0}^{+\infty} \frac{1}{l!} x^L (\partial_L \delta u)(\mathbf{0})\,. \tag{B1}$$

Here the derivative operator ∂_L is a priori non-STF, but we can decompose it into a sum of STF components using the formula (see appendix A of Blanchet & Damour 1986 for a compendium of useful formulae):

$$\partial_L = \sum_{k=0}^{[l/2]} a_k^l\, \delta_{(2K}\, \hat{\partial}_{L-2K)}\, \Delta^k\,, \tag{B2}$$

where k ranges from 0 to the integer part of $l/2$, denoted by $[l/2]$, where δ_{2K} denotes a product of k Kronecker symbols carrying $2k$ indices chosen from among those of $L = i_1 \ldots i_l$, where the parenthesis indicates full symmetrization over the l indices, $i_1 \ldots i_l$, where $\Delta \equiv \partial_{ii}$ denotes the ordinary Laplacian and where the coefficients depending on l and k are given by

$$a_k^l = \frac{l!}{(l-2k)!}\frac{(2l-4k+1)!!}{(2k)!!(2l-2k+1)!!}\,. \tag{B3}$$

Now using the fact that $\Delta\delta u = 0$ in a neighbourhood of the origin ($r \leq \varepsilon$), we see that only the term $k = 0$ will survive in the latter sum and since $a^l_{k=0} = 1$, we conclude that we can replace in fact the derivative operator in $(\partial_L\, \delta u)(\mathbf{0})$ by its STF projection $\hat{\partial}_L$; hence,

$$\delta u = \sum_{l=0}^{+\infty} \frac{1}{l!} x^L (\hat{\partial}_L \delta u)(\mathbf{0})\,. \tag{B4}$$

Next, we prove that the contribution from the Newtonian potential, u_N, in equation (B4) is purely monopolar. This comes from our assumption that the density of ordinary matter ρ in the Sun is both regular (i.e. C^∞) and spherically symmetric, that is, depending only on r (neglecting the back-reaction of the field on its source). As we will now prove, this means that the Taylor expansion of $\rho(r)$ in spherical symmetry must contain only even powers of r. The density being regular its expansion when $r \to 0$ is given by Taylor's formula as

$$\rho = \sum_{l=0}^{+\infty} \frac{1}{l!} x^L (\partial_L \rho)(\mathbf{0})\,. \tag{B5}$$

Next, we again use formula (B2) to decompose equation (B5) into a sum of STF pieces. Because ρ is spherically symmetric, all these STF pieces must be zero except the monopolar contribution; hence, only the terms for which $l = 2k$ survive in the latter decomposition. Using the value of the coefficient $a_k^{2k} = 1/(2k+1)$, we are then left with

$$\rho = \sum_{k=0}^{+\infty} \frac{r^{2k}}{(2k+1)!}\,(\Delta^k \rho)(\mathbf{0})\,. \tag{B6}$$

As we see, $\rho(r)$ admits an expansion containing only even powers of r. Now the spherically-symmetric Newtonian potential, u_N, will also admit an expansion only in even powers of r, so we write, accordingly, $u_\mathrm{N}(r) = f(r^2)$. Acting on a function of r^2, the STF derivative operator gives $\hat{\partial}_L f(r^2) = \hat{n}^L (2r)^l f^{(l)}(r^2)$, where $f^{(l)}$ denotes the lth derivative of this function (see Blanchet & Damour 1986). Hence, we find that $\hat{\partial}_L u_\mathrm{N}$ is a perfectly regular function and we conclude that $(\hat{\partial}_L u_\mathrm{N})(\mathbf{0}) = 0$ except for the monopole case $l = 0$. We can therefore replace $(\hat{\partial}_L \delta u)(\mathbf{0})$ in equation (B4) by $(\hat{\partial}_L u)(\mathbf{0})$ for any $l \geq 1$ and we have finally established the result

$$\delta u = -u_\mathrm{N}(\mathbf{0}) + \sum_{l=0}^{+\infty} \frac{1}{l!} x^L (\hat{\partial}_L u)(\mathbf{0}), \tag{B7}$$

which is the same as in equation (19).

This paper has been typeset from a TEX/LATEX file prepared by the author.